Mon. Not. R. astr. Soc. (1989) **238,** 1319–1343

Spatial distribution and dynamics of the galactic globular cluster system

Peter Thomas *Canadian Institute for Theoretical Astrophysics, 60 St George St., Toronto, Ontario M5S 1A1, Canada*

Accepted 1988 October 18. Received 1988 October 1; in original form 1988 July 30

Summary. We use relatively complete datasets from the literature to investigate the spatial and velocity distribution of the galactic globular cluster system. The sky positions appear circularly symmetric about the Galactic Centre and can be used to constrain the spatial distribution. Distance errors are large – modelling suggests a variance in the distance modulus of about 0.5 mag. Rotation of the globular cluster system is only weakly constrained; the best-fit rotation velocity decreases at large radii but the data are consistent with either a constant or Keplerian rotation curve. Metal-rich clusters are flattened towards the galactic plane and show a slight tendency to rotate faster and to have a lower velocity dispersion than the mean population. The velocity ellipsoid appears isotropic inside the solar radius but much of this effect could be due to distance errors. The line of sight velocity dispersion increases beyond 7 kpc but since the orbits may become more radial this provides only a weak constraint on the galactic mass. Models of the velocity dispersion lead to galactic circular speeds of between about 180 and 220 km s^{-1} at the solar radius, which may either rise, remain constant or even decrease at large radii.

1 Introduction

In this paper we examine the spatial and velocity distributions of the globular cluster system of the Galaxy and investigate the constraints they impose on the mass of the Galaxy. Various aspects of this problem have been investigated many times in the past (e.g. Mayall 1946; Kinman 1959; Hartwick & Sargent 1978; Frenk & White 1980). We extend these analyses to a much larger dataset and discuss the size of distance errors and their effect on our conclusions.

There now exist relatively complete catalogues of the distances, metallicities and radial velocities of the known galactic globular clusters. These are compiled from a wide variety of sources and sometimes contain large errors but the data are unlikely to improve substantially for some time. It is shown in Section 3 that there are no signs of extensive incompleteness due to obscuration. The sky distribution can be used to infer the space density of the clusters but the errors in the distance estimates, which may be as much as a factor of two, cast doubt on any results which depend strongly upon the three-dimensional positions. The rotation velocity of the cluster system is investigated in Section 4. Monte Carlo simulations show that the results

are not strongly affected by the errors, but the statistics are such that the constraints are weak; the data are adequately explained by a rotation speed which is constant or decreases outward. The line of sight velocity dispersion, discussed in Section 5, shows a large increase outside the solar radius. This observation led Frenk & White (1980) to conclude that the rotation curve of the Galaxy must be flat or rising to large radii. However, the shape of the velocity ellipsoid is not well constrained and models which become strongly radial at large radii are found; these can give circular speeds which decrease at large radii. Even though the line of sight velocity is increasing, the resulting constraints on the mass of the Galaxy are poor.

The metal-rich and metal-poor globular clusters have different spatial and velocity distributions but it is not clear whether they form distinct populations or whether there is a gradual transition between the two. The metallicity data used here are inadequate to resolve this issue and the reader is referred to the work of Zinn (1985) and Armandroff & Zinn (1988) for a fuller discussion.

2 Preliminaries

2.1 DATA

We try to use as large and homogeneous a sample as possible. The basic dataset of 153 globular clusters is taken from Webbink (1985, hereafter W85). This lists positions, distances and metallicities along with the methods used in the derivations and the associated uncertainties. UKS 2, which is probably not a globular cluster (W85; Armandroff & Zinn 1988, hereafter AZ88), has not been included. Of these clusters 147 have distance estimates, derived by assuming an absolute magnitude for the horizontal branch of 0.6. The major uncertainty comes from the measurement of reddening and the associated absorption, especially for clusters near the galactic plane and towards the Galactic Centre. Metallicities are derived from the colours of the subgiant branch after dereddening. Once again there is considerable uncertainty as can be seen by comparing the estimates in W85 and Zinn (1985, hereafter Z85). We use the values in W85 (the metallicity of Ter 6 is from AZ88) to compare with the work of Zinn and to show that it is important to have a well-observed and homogeneous sample in order to confirm Zinn's results. In the following 'metal-poor' and 'metal-rich' mean [Fe/H] < -1.0 and > -1.0, respectively.

Radial velocities are taken from the extensive survey of Hesser, Shawl & Meyer (1986, hereafter HSM). Where they did not observe a globular cluster themselves (or for NGC 6356 where their observation was a poor one) the value listed in their table as being from Webbink (1981) was used or, failing this, the value was taken from AZ88. This gives a total of 115 clusters with velocities. HSM compare their results with previous surveys and find that in general the agreement is to within about 40 km s^{-1} although there are a few exceptions in which the discrepancy exceeds 100 km s^{-1}.

The data are listed in Table 1.

2.2 COORDINATES

The coordinate system is summarized in Fig. 1. The angle between the Galactic Centre and the position of the globular cluster is ω, where

$$\cos\omega = \cos b \cos l \tag{1}$$

and the angular displacement of the great circle on the sky containing the cluster and the Galactic Centre from the plane of the Galaxy is θ, where

$$\tan\theta = |\tan b \csc l|. \tag{2}$$

Table 1. Data and derived parameters for the globular clusters. The columns contain the name (see W85 for an explanation of terms), galactic longitude and latitude, distance (kpc), heliocentric velocity (km s^{-1}), metallicity, angular displacement from the Galactic Centre, angular displacement from the galactic plane, derived distances in the x, y and z directions, distance from the Galactic Centre and velocity relative to the local standard of rest.

name	l	b	r	v_{obs}	Z	ω	θ	x	y	z	R	v
N 104	305.895	-44.889	4.6	-22.	-0.75	65.	51.	1.9	-2.6	-3.2	6.6	-158.
N 288	151.147	-89.377	8.2	-48.	-1.39	91.	90.	-0.1	0.0	-8.2	10.9	-54.
N 362	301.533	-46.247	8.7	217.	-1.39	69.	51.	3.1	-5.1	-6.3	9.0	76.
N 1261	270.539	-52.127	16.1	51.	-1.17	90.	52.	0.1	-9.9	-12.7	17.5	-99.
Pal 1	130.967	19.023	13.7	3.	-1.01	128.	25.	-8.5	9.8	4.5	18.9	167.
N 1466	286.700	-39.537	39.4		-2.15	77.	41.	8.7	-29.1	-25.1	38.5	
AM 1	258.360	-48.472	116.4		-1.68	98.	49.	-15.6	-75.6	-87.1	117.6	
Eri	218.108	-41.331	84.7	-41.	-1.22	126.	55.	-50.0	-39.3	-55.9	89.0	-161.
Ret	268.664	-40.269	50.4		-2.01	91.	40.	-0.9	-38.4	-32.6	51.0	
Pal 2	170.532	-9.070	13.6	-133.	-1.68	167.	44.	-13.2	2.2	-2.1	20.5	-106.
N 1841	297.016	-30.147	40.9		-1.56	67.	33.	16.1	-31.5	-20.5	38.7	
N 1851	244.512	-35.036	12.0	306.	-1.25	111.	38.	-4.2	-8.9	-6.9	15.9	124.
N 1904	227.231	-29.350	13.0	193.	-1.47	126.	37.	-7.7	-8.3	-6.4	18.1	33.
N 2298	245.629	-16.007	10.6	108.	-2.06	113.	17.	-4.2	-9.3	-2.9	14.9	-104.
N 2419	180.370	25.242	91.4	-20.	-1.98	155.	89.	-82.7	-0.5	39.0	97.8	-27.
AM 2	248.126	-5.876	57.7			112.	6.	-21.4	-53.3	-5.9	60.7	
N 2808	282.193	-11.252	9.5	98.	-1.47	78.	12.	2.0	-9.1	-1.9	10.6	-127.
E 3	292.269	-19.018	8.3		-0.96	69.	20.	3.0	-7.3	-2.7	8.8	
Pal 3	240.142	41.866	87.9	22.	-1.68	112.	46.	-32.6	-56.8	58.7	90.8	-129.
N 3201	277.229	8.641	5.0	477.	-1.60	83.	9.	0.6	-4.9	0.8	8.1	248.
ESO 09	293.508	-4.041	59.5			67.	4.	23.7	-54.4	-4.2	57.1	
Pal 4	202.293	71.801	93.3	168.	-1.30	107.	83.	-27.0	-11.1	88.6	95.6	144.
N 4147	252.848	77.189	17.3	177.	-1.68	94.	78.	-1.1	-3.7	16.9	19.1	134.
N 4372	300.995	-9.881	4.9	49.	-1.77	60.	11.	2.5	-4.1	-0.8	6.2	-146.
Rup106	300.888	11.670	26.7			60.	14.	13.4	-22.4	5.4	23.9	
N 4590	299.625	36.051	9.6	-84.	-1.85	66.	40.	3.8	-6.7	5.6	9.4	-241.
N 4833	303.604	-8.014	5.8	194.	-1.98	57.	10.	3.2	-4.8	-0.8	6.2	4.
N 5024	332.965	79.764	18.5	-80.	-1.89	81.	85.	2.9	-1.5	18.2	18.7	-90.
N 5053	335.675	78.946	15.8		-2.02	80.	85.	2.8	-1.2	15.5	16.1	
N 5139	309.100	14.971	5.2	222.	-1.60	52.	19.	3.2	-3.9	1.3	5.7	53.
N 5272	42.218	78.707	10.4	-141.	-1.30	82.	82.	1.5	1.4	10.2	11.7	-101.
N 5286	311.614	10.568	9.7	58.	-1.60	49.	14.	6.3	-7.1	1.8	7.4	-107.
AM 4	320.280	33.506	30.3		-2.23	50.	46.	19.4	-16.1	16.7	26.3	
N 5466	42.137	73.593	15.8	120.	-1.85	78.	79.	3.3	3.0	15.2	15.9	174.
N 5634	342.210	49.260	25.0	-41.	-1.77	52.	75.	15.5	-5.0	18.9	21.3	-76.
N 5694	331.056	30.360	31.3	-152.	-1.89	41.	50.	23.6	-13.1	15.8	26.4	-239.
I 4499	307.354	-20.473	18.0		-1.77	55.	25.	10.2	-13.4	-6.3	15.1	
N 5824	332.555	22.071	24.6	-38.	-1.98	35.	41.	20.2	-10.5	9.2	19.2	-127.
Pal 5	0.847	45.853	21.4		-1.43	46.	89.	14.9	0.2	15.4	17.2	
N 5897	342.948	30.294	11.8	23.	-1.47	34.	63.	9.7	-3.0	6.0	7.2	-25.
N 5904	3.860	46.797	7.6	52.	-1.60	47.	86.	5.2	0.4	5.5	5.9	75.
N 5927	326.605	4.859	8.8	-106.	-0.67	34.	9.	7.3	-4.8	0.7	4.9	-226.
N 5946	327.582	4.192	9.2	127.	-1.34	33.	8.	7.7	-4.9	0.7	5.0	10.
BH 176	328.417	4.344	85.7			32.	8.	72.8	-44.8	6.5	79.8	
N 5986	337.028	13.273	10.5	94.	-1.72	26.	31.	9.4	-4.0	2.4	5.2	15.
Pal 14	28.755	42.177	75.3		-1.34	49.	62.	48.9	26.8	50.6	70.9	
N 6093	352.674	19.462	8.0	4.	-2.15	21.	70.	7.5	-1.0	2.7	2.9	-12.
N 6101	317.751	-15.828	16.1	206.	-1.68	45.	23.	11.5	-10.4	-4.4	12.1	59.
N 6121	350.975	15.974	2.1	61.	-1.09	18.	61.	2.0	-0.3	0.6	5.1	37.
N 6144	351.929	15.702	9.5	162.	-1.81	18.	63.	9.1	-1.3	2.6	3.5	142.
N 6139	342.365	6.939	8.1	4.	-1.60	19.	22.	7.7	-2.4	1.0	2.7	-56.
Ter 3	345.083	9.190	27.2			17.	32.	25.9	-6.9	4.3	20.6	
N 6171	3.371	23.012	6.2	-22.	-0.88	23.	82.	5.7	0.3	2.4	2.8	3.
ESO 45	351.912	12.097	10.3		-1.01	15.	57.	10.0	-1.4	2.2	3.9	

Table 1 – *continued*

name	l	b	r	v_{obs}	Z	ω	θ	x	y	z	R	v
N 6205	59.006	40.914	7.1	-248.	-1.61	67.	45.	2.8	4.6	4.6	7.8	-87.
N 6218	15.715	26.313	5.3	-44.	-1.89	30.	61.	4.6	1.3	2.3	3.6	25.
N 6229	73.638	40.306	31.6	-154.	-1.39	78.	41.	6.8	23.1	20.4	30.9	25.
N 6235	358.918	13.520	9.5	86.	-1.60	14.	86.	9.2	-0.2	2.2	3.1	93.
N 6254	15.138	23.074	4.5	76.	-1.51	27.	58.	4.0	1.1	1.8	3.7	144.
N 6256	347.791	3.307	9.1		-1.56	13.	15.	8.9	-1.9	0.5	2.7	
Pal 15	18.873	24.293	69.7		-1.26	30.	54.	60.1	20.5	28.7	63.7	
N 6266	353.575	7.317	6.1	-78.	-1.26	10.	49.	6.0	-0.7	0.8	1.5	-93.
N 6273	356.869	9.381	10.6	131.	-2.40	10.	72.	10.4	-0.6	1.7	3.8	129.
N 6284	358.347	9.939	10.3	41.	-1.34	10.	81.	10.1	-0.3	1.8	3.6	46.
N 6287	0.132	11.023	7.2	-208.	-1.72	11.	89.	7.1	0.0	1.4	1.4	-196.
N 6293	357.620	7.834	7.7	-143.	-1.85	8.	73.	7.6	-0.3	1.0	1.2	-142.
TJ 5	357.261	7.283				8.	69.					
N 6304	355.825	5.374	6.0	-102.	-0.54	7.	52.	6.0	-0.4	0.6	1.3	-108.
N 6316	357.175	5.765	12.8	76.	-0.62	6.	64.	12.7	-0.6	1.3	5.8	75.
N 6325	0.973	8.003	6.2	8.	-2.02	8.	83.	6.1	0.1	0.9	1.3	23.
TJ 16	357.713	5.636				6.	68.					
TJ 15	358.939	6.468				7.	81.					
TJ 17	357.688	5.564				6.	68.					
N 6341	68.339	34.858	7.7	-120.	-1.89	72.	37.	2.3	5.9	4.4	8.7	67.
N 6333	5.544	10.705	7.5	260.	-1.77	12.	63.	7.3	0.7	1.4	1.6	294.
N 6342	4.899	9.725	11.6	84.	-0.75	11.	64.	11.4	1.0	2.0	4.9	115.
N 6356	6.723	10.220	16.7	32.	-1.17	12.	57.	16.3	1.9	3.0	9.9	70.
N 6355	359.585	5.428	7.1	-184.	-1.34	5.	86.	7.1	-0.1	0.7	0.7	-175.
N 6352	341.421	-7.164	6.6	-118.	-0.07	20.	22.	6.2	-2.1	-0.8	2.4	-184.
Ter 2	356.320	2.298	10.0	109.	-0.54	4.	32.	10.0	-0.6	0.4	3.0	104.
N 6366	18.411	16.041	4.0		-0.71	24.	42.	3.6	1.2	1.1	3.8	
N 6362	325.555	-17.569	7.7	-15.	-0.71	38.	29.	6.1	-4.2	-2.3	4.9	-136.
Ter 4	356.024	1.308	16.1	-50.	-0.29	4.	18.	16.1	-1.1	0.4	9.1	-56.
HP 1	357.423	2.113	9.5	44.	-1.68	3.	39.	9.5	-0.4	0.4	2.5	44.
Gri 1	354.304	-0.151	11.8			6.	2.	11.7	-1.2	0.0	4.8	
Lil 1	354.841	-0.161	7.9	52.	-0.29	5.	2.	7.9	-0.7	0.0	1.1	41.
N 6380	350.182	-3.414	4.0		-1.30	10.	19.	3.9	-0.7	-0.2	3.2	
Ter 1	357.558	0.992	10.6	35.	0.10	3.	22.	10.6	-0.5	0.2	3.6	35.
N 6388	345.557	-6.738	13.5	77.	-0.62	16.	25.	13.0	-3.3	-1.6	7.0	27.
Ton 2	350.797	-3.419	8.7			10.	20.	8.6	-1.4	-0.5	2.1	
N 6402	21.322	14.803	10.2	-25.	-2.19	26.	36.	9.2	3.6	2.6	4.9	69.
N 6401	3.451	3.978	7.1	-62.	-1.01	5.	49.	7.1	0.4	0.5	0.7	-37.
N 6397	338.165	-11.959	2.2	2.	-2.02	25.	30.	2.0	-0.8	-0.5	5.1	-76.
Pal 6	2.092	1.779	5.9		0.22	3.	40.	5.9	0.2	0.2	1.2	
TJ 23	356.676	-1.916				4.	30.					
N 6426	28.088	16.233	17.5	-162.	-1.94	32.	32.	14.8	7.9	4.9	12.1	-45.
Ter 5	3.838	1.687	7.1	-94.	-0.71	4.	24.	7.1	0.5	0.2	0.5	-68.
N 6440	7.729	3.800	7.1	-83.	-0.54	9.	26.	7.0	1.0	0.5	1.1	-41.
N 6441	353.532	-5.006	11.7	20.	-0.07	8.	38.	11.6	-1.3	-1.0	4.8	3.
N 6453	355.717	-3.873	10.7	-84.	-1.51	6.	42.	10.6	-0.8	-0.7	3.8	-92.
Ter 6	358.572	-2.163	12.8	126.	-0.61	3.	57.	12.8	-0.3	-0.5	5.8	130.
UKS 1	5.125	0.764	10.4		-1.22	5.	8.	10.4	0.9	0.1	3.4	
N 6496	348.026	-10.012	6.3	-95.	-0.71	16.	40.	6.1	-1.3	-1.1	2.0	-135.
Ter 9	3.603	-1.988	7.0	58.	-0.45	4.	29.	7.0	0.4	-0.2	0.5	83.
N 6517	19.225	6.762	6.1	-37.	-1.47	20.	20.	5.7	2.0	0.7	2.5	50.
Ter 10	4.421	-1.864	14.6			5.	23.	14.5	1.1	-0.5	7.6	
N 6522	1.026	-3.929	6.6	-11.	-1.56	4.	75.	6.6	0.1	-0.5	0.7	3.
N 6535	27.176	10.435	6.9	-159.	-1.56	29.	22.	6.0	3.1	1.2	3.5	-43.
N 6528	1.138	-4.175	6.8	160.	-0.96	4.	75.	6.8	0.1	-0.5	0.6	174.
N 6539	20.795	6.775	3.1	-52.	-1.05	22.	19.	2.9	1.1	0.4	4.3	41.
N 6544	5.837	-2.201	2.6	2.	-2.15	6.	21.	2.6	0.3	-0.1	4.5	36.
N 6541	349.286	-11.189	7.0	-158.	-2.02	15.	47.	6.7	-1.3	-1.4	1.9	-193.

Table 1 – *continued*

name	l	b	r	v_{obs}	Z	ω	θ	x	y	z	R	v
N 6553	5.253	-3.029	5.7	-24.	-0.41	6.	30.	5.7	0.5	-0.3	1.5	7.
N 6558	0.200	-6.024	8.8	-146.	-1.51	6.	88.	8.8	0.0	-0.9	1.9	-136.
Pal 7	21.832	5.666	9.8		-0.84	23.	15.	9.1	3.6	1.0	4.3	
Ter 11	8.357	-2.100	23.7			9.	14.	23.4	3.4	-0.9	16.8	
N 6569	0.481	-6.681	8.9	-26.	-1.01	7.	86.	8.8	0.1	-1.0	2.1	-15.
Kod 1	18.072	2.415				18.	8.					
N 6584	342.144	-16.413	15.0	235.	-1.56	24.	44.	13.7	-4.4	-4.2	9.0	173.
N 6624	2.788	-7.913	8.0	55.	-0.84	8.	71.	7.9	0.4	-1.1	1.5	75.
N 6626	7.799	-5.580	5.8	-2.	-1.81	10.	36.	5.7	0.8	-0.6	1.6	39.
N 6638	7.897	-7.153	6.7	24.	-0.92	11.	42.	6.6	0.9	-0.8	1.3	65.
N 6637	1.722	-10.269	10.3	31.	-0.92	10.	81.	10.1	0.3	-1.8	3.6	47.
N 6642	9.814	-6.439	5.5	-47.	-1.30	12.	34.	5.4	0.9	-0.6	2.0	2.
N 6652	1.535	-11.377	14.3	-80.	-0.92	11.	82.	14.0	0.4	-2.8	7.5	-65.
N 6656	9.890	-7.552	3.1	-164.	-1.81	12.	38.	3.0	0.5	-0.4	4.1	-115.
Pal 8	14.103	-6.797	28.1	-38.	-0.50	16.	26.	27.1	6.8	-3.3	21.4	28.
N 6681	2.853	-12.510	9.3	223.	-0.92	13.	77.	9.1	0.5	-2.0	2.9	243.
N 6712	25.353	-4.318	6.2	-81.	-1.26	26.	10.	5.6	2.6	-0.5	3.1	28.
N 6715	5.607	-14.088	21.5	133.	-1.85	15.	69.	20.8	2.0	-5.2	14.8	163.
N 6717	12.876	-10.901	7.8	-6.	-2.19	17.	41.	7.5	1.7	-1.5	2.3	54.
N 6723	0.072	-17.298	9.2	-79.	-1.09	17.	90.	8.8	0.0	-2.7	3.2	-71.
N 6749	36.201	-2.204	12.8		-0.37	36.	4.	10.3	7.6	-0.5	8.2	
N 6752	336.495	-25.628	4.1	-15.	-1.64	34.	50.	3.4	-1.5	-1.8	4.3	-95.
N 6760	36.108	-3.924	4.1	-28.	-0.84	36.	7.	3.3	2.4	-0.3	4.5	118.
Ter 7	3.387	-20.063	36.4			20.	81.	34.1	2.0	-12.5	29.9	
N 6779	62.659	8.336	9.8	-138.	-2.32	63.	9.	4.5	8.6	1.4	9.1	75.
Pal 10	52.437	2.726	10.6			52.	3.	6.5	8.4	0.5	8.4	
Arp 2	8.543	-20.787	28.3		-1.85	22.	69.	26.2	3.9	-10.0	21.9	
N 6809	8.798	-23.272	5.1	159.	-1.56	25.	70.	4.6	0.7	-2.0	3.2	198.
Ter 8	5.758	-24.558	48.2			25.	78.	43.6	4.4	-20.0	41.9	
Pal 11	31.806	-15.577	13.8	-68.	-0.92	35.	28.	11.3	7.0	-3.7	9.0	58.
N 6838	56.742	-4.562	4.4	-41.	-0.45	57.	5.	2.4	3.7	-0.3	5.9	160.
N 6864	20.304	-25.748	18.5	-175.	-1.68	32.	54.	15.6	5.8	-8.0	13.1	-96.
N 6934	52.105	-18.894	14.9	-387.	-1.30	54.	23.	8.7	11.1	-4.8	12.2	-208.
N 6981	35.163	-32.683	17.0	-309.	-1.56	47.	48.	11.7	8.2	-9.2	13.2	-192.
N 7006	63.769	-19.407	39.1	-364.	-1.72	65.	21.	16.3	33.1	-13.0	36.7	-163.
N 7078	65.013	-27.313	9.7	-100.	-2.06	68.	30.	3.6	7.8	-4.5	9.6	90.
N 7089	53.371	-35.770	11.9	-5.	-1.81	61.	42.	5.8	7.7	-7.0	10.5	149.
N 7099	27.179	-46.835	7.2	-160.	-2.19	53.	67.	4.4	2.2	-5.3	6.3	-86.
Pal 12	30.510	-47.680	19.4	9.	-1.13	55.	65.	11.3	6.6	-14.3	16.4	90.
Pal 13	87.104	-42.699	24.4	-28.	-0.96	88.	43.	0.9	17.9	-16.5	25.1	140.
N 7492	53.392	-63.479	19.1	-189.	-1.81	75.	68.	5.1	6.8	-17.1	18.5	-109.

Both these angles depend only upon the position of the cluster on the sky and so are well determined. If, in addition, the distance, r, is known then the position in Cartesian coordinates x, y and z, centred on the Sun, can be evaluated. The x-axis points towards the Galactic Centre ($l=0°$, $b=0°$), the y-axis in the direction ($l=90°$, $b=0°$) and the z-axis towards the north galactic pole ($b=90°$):

$$x = r\cos b\cos l$$

$$y = r\cos b\sin l \qquad (3)$$

$$z = r\sin b.$$

Taking the distance to the Galactic Centre to be g and denoting galactocentric coordinates with capital letters gives

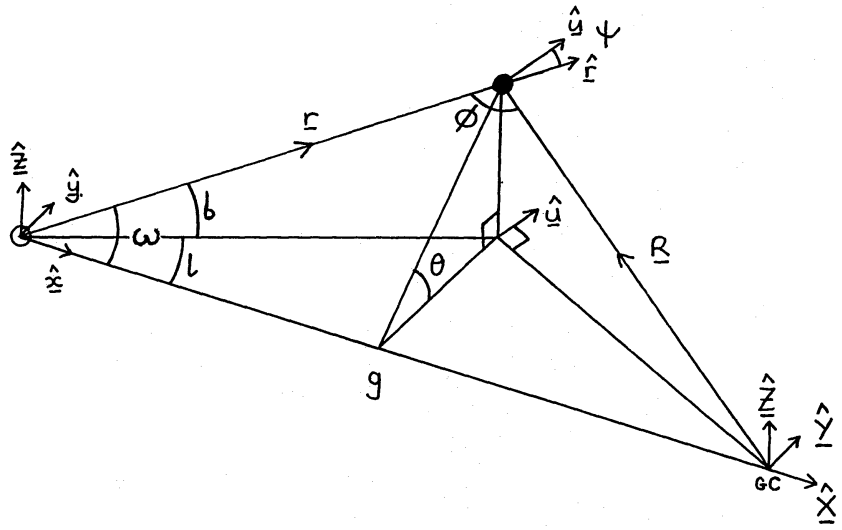

Figure 1. The coordinate systems used in this paper.

$$X = x - g$$
$$Y = y \tag{4}$$
$$Z = z$$
$$R = \sqrt{X^2 + Y^2 + Z^2}.$$

Two other angles which turn out to be useful are ϕ – the angle between the line-of-sight and the radius vector from the Galactic Centre,

$$\cos\phi = \hat{\mathbf{r}} \cdot \hat{\mathbf{R}} = \frac{R^2 + gX}{rR}, \tag{5}$$

and ψ – the angle between the line-of-sight and the rotation vector about a vertical axis through the Galactic Centre (in a negative sense – see Fig. 1),

$$\cos\psi = \hat{\mathbf{r}} \cdot \hat{\mathbf{u}} = \frac{gY}{r\sqrt{X^2 + Y^2}}. \tag{6}$$

2.3 STATISTICS

In Section 3 the Kolmogorov–Smirnov (KS) test is used to check whether two distributions may have been drawn from the same parent distribution. If the distributions contain n_1 and n_2 clusters then the disagreement is measured by $\delta = \sqrt{n_1 n_2/(n_1 + n_2)}\Delta$, where Δ is the maximum difference between the cumulative frequencies. For large n_1, $n_2 (\gtrsim 30)$, values of $\delta = 1.22$ and 1.36 indicate, respectively, 90 and 95 per cent probabilities that the null hypothesis of the same parent distribution may be rejected. When comparing a single distribution of n points against a model the appropriate value of $\delta = \sqrt{n}\Delta$.

The KS test has the advantages of being both model independent and tolerant of gaps and errors in the data. It is also much easier to apply than a χ^2 test as it does not require binning of the data, however it is not always so powerful at detecting deviations near the end-points of a distribution.

We also use the KS test to determine the allowable range of parameters in fits to the spatial distribution of the globular cluster system. These are varied until the fit becomes unacceptable at 90 per cent confidence; this approach is reasonable because the best-fit models do describe the data well.

In Sections 4 and 5 the Spearman rank-order coefficient, S, is used to detect correlations between residuals in the data (after 'subtraction' of the model) and independent variables such as radius or $\cos\psi$. Models are rejected if a residual trend is detected at greater than 90 per cent confidence. For large n, $S\sqrt{(n-2)/(1-S^2)}$ is distributed as a student-t distribution with $n-2$ degrees of freedom.

It can be seen from Fig. 8 that R and $\cos^2\phi$ are strongly correlated, however this is simply due to a lack of points with a small value of $\cos^2\phi$ at $R \gtrsim 7$ kpc and not to a true linear dependence between the variables. Frenk & White (1980) combine the correlation coefficients over R and $\cos^2\phi$ to form a joint coefficient for the overall distribution. We find that this can give constraints which are stronger, intermediate or even weaker than those obtained by treating correlations with the independent variables separately; for this reason we choose not to use this statistic here. In any case it is often more instructive to look for correlations within restricted subsamples of the data, which can be obscured when considering the data as a whole.

2.4 TEST DATASETS

For the models used in Sections 4 and 5 it is not clear whether the formal errors in the parameter range reflect the real uncertainties; this is especially true because of the large distance errors reported in Section 3. For this reason test datasets were created and analysed in the same way as the real data. In each case 120 points were chosen with a spatial distribution resembling that found in Section 3. These were given a constant rotation velocity of 100 km s^{-1} and either a radial, tangential or isotropic velocity dispersion with one-dimensional root mean square components of 100 km s^{-1}. In addition distance errors were included where required. In each case 100 datasets were generated and analysed; the mean and standard deviation of the results were then used as indications of the errors.

3 Spatial distribution

3.1 PROJECTED DISTRIBUTION ON THE SKY

Fig. 2 shows the globular cluster sample projected on to the sky. There is no departure from azimuthal symmetry such as might be expected if there were significant obscuration near the galactic plane. To test for this we plot in Fig. 3 the number of clusters with $\theta \leq \Theta$ against Θ. There is a greater than 80 per cent chance on a KS test that a deviation of this size or larger would be obtained if the data were drawn from a uniform distribution over Θ. Suppose that the true distribution is ellipsoidal with axial ratio ε (where $\varepsilon < 1$ represents a 'squashing' along the z-axis). Then the observed angle θ is related to the unsquashed angle θ' by $\tan\theta = \varepsilon\tan\theta'$. θ' is uniformly distributed giving a number distribution $n(<\theta) = N[2/\pi\tan^{-1}(\varepsilon^{-1}\tan\theta)]$, where N is the total number. This gives a 90 per cent confidence range for the globular cluster sample of $0.72 < \varepsilon < 1.15$. If obscuration is important then the true value of ε will be lower.

The lack of flattening of the globular cluster population as a whole is consistent with the conclusions of Frenk & White (1982, hereafter FW82) and Z85. However, it has been strongly suggested by Zinn that the metal-rich clusters form a highly flattened, disc-like system. FW82 found little evidence for this in those clusters with [Fe/H] > -1.2 and $|b| > 5.7°$ although, as

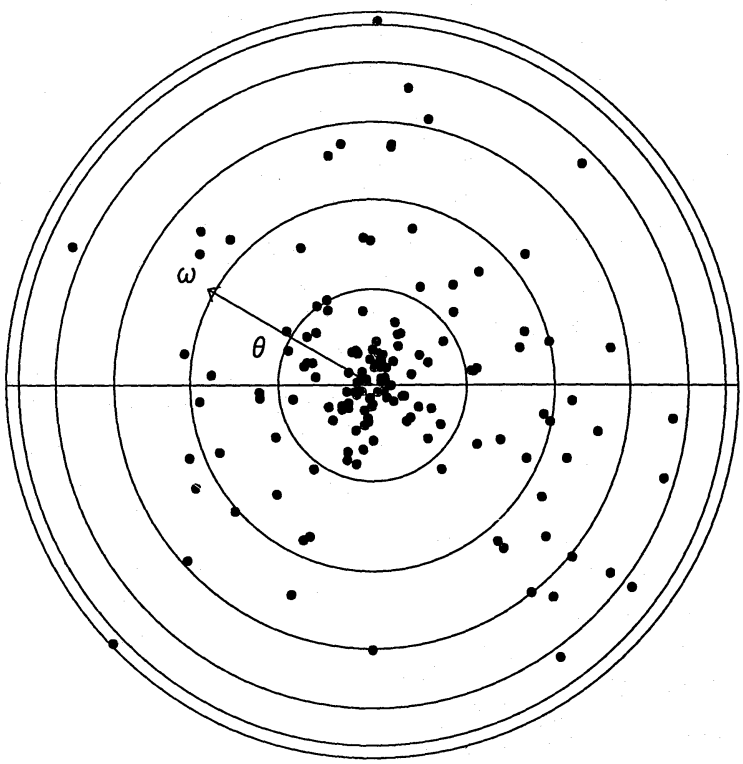

Figure 2. The globular cluster sample projected on to the sky. The scale is chosen so as to give an equal area projection centred on the Galactic Centre – the circles are spaced at intervals of 30° in ω.

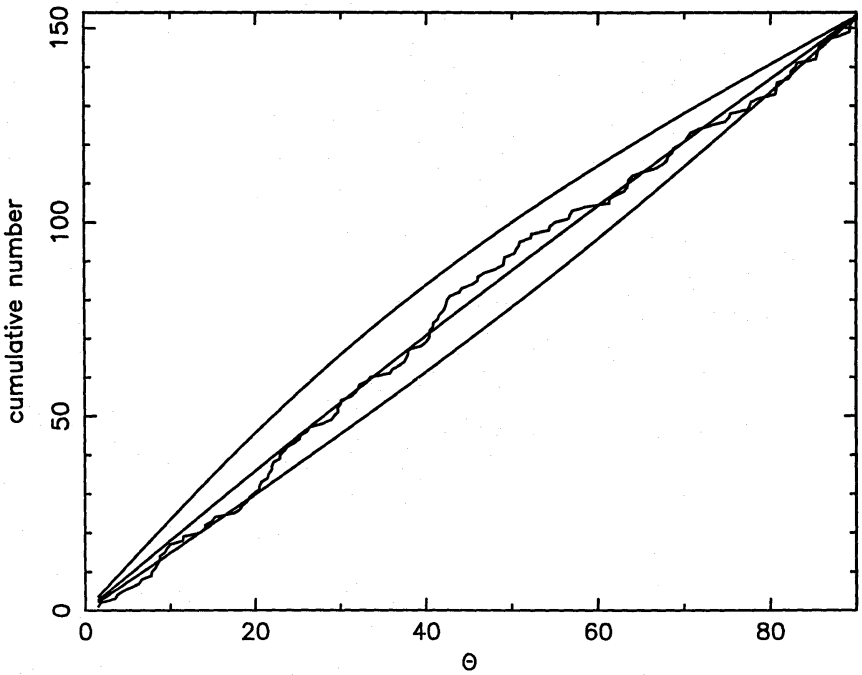

Figure 3. The number of clusters with angular displacement from the galactic plane less than θ, plotted against θ. The sample is consistent with being drawn from a uniform distribution; the outer lines show the 90 per cent bounds on the underlying distribution.

they themselves realized, the very nature of this analysis makes it difficult to detect a highly flattened system. Fig. 4 shows the sky distribution of metal-rich clusters. The best-fit value of ε is 0.66 with 90 per cent confidence range $0.47 < \varepsilon < 0.95$. This represents a flattening similar

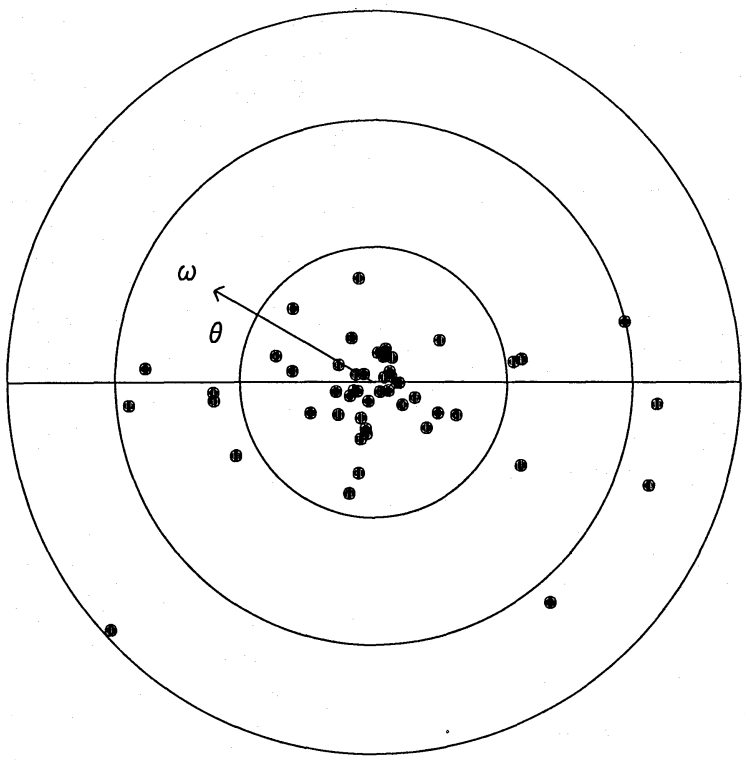

Figure 4. Projected distribution on the sky of the metal-rich globular clusters. Note that of the two clusters which appear furthest from the galactic plane, one (NGC 104) is nearby and actually lies just 3.2 kpc from the plane, the other (Pal 3) has an uncertain metallicity and the value of [Fe/H] = −1.75 given in Z85 would place it well within the metal-poor subsample.

to that reported by Z85 who used a higher metallicity cut of [Fe/H] > −0.8. The metal-poor clusters are uniformly distributed except that there are none with $\Theta < 6°$ whereas seven would have been expected. This may be evidence for incompleteness of the sample due to obscuration, but note that four out of the 18 clusters without metallicity determinations also lie in this range.

There are large differences in the metallicities reported by W85 and Z85: over half the metal-rich clusters differ in [Fe/H] by more than 0.2 and some by over 1. The difficulty is that of measuring metallicity in heavily reddened systems. Recent work by AZ88 uses the Ca II infrared triplet to overcome this problem but as yet they have applied this technique to only a small sample of clusters; a larger dataset obtained using this technique would be of great value. Freeman & Norris (1981), Z85 and AZ88 all find a bimodality in the distribution of clusters over metal abundance, however such a division is not present in Webbink's compilation. The spatial distribution and kinematics do differ between the metal-rich and metal-poor subsystems but the transition could be gradual rather than abrupt. Clearly a large, homogeneous and accurate dataset is needed in order to address this problem. We treat the metal-rich and metal-poor data together, except where stated otherwise.

By assuming that the globular cluster population is spherically symmetric about the Galactic Centre, the sky distribution can be used to infer the three-dimensional distribution. FW82 used Monte Carlo simulations to investigate this question; we instead consider a family of analytic models with space density $\rho \propto [1+(R/a)^2]^{-s/2}$, where a is the core radius and s the asymptotic slope of the density at large radii. These give projected distributions at angles less than ω from the Galactic Centre of

$$n(<\omega)=\frac{N}{2}\left[\left(1+\frac{I_{s-4}(X_\odot)}{I_{s-4}(\infty)}\right)\right. \tag{7}$$

$$\left.-\cos\omega(1+X_\odot^2\sin^2\omega)^{(3-s)/2}\left(1+\frac{I_{s-4}(X_\odot\cos\omega(1+X_\odot^2\sin^2\omega)^{-1/2})}{I_{s-4}(\infty)}\right)\right],$$

where $X_\odot = g/a$ and

$$I_\alpha(X)=\int_0^X\frac{du}{(1+u^2)^{1+\alpha/2}}=\int_0^{\tan^{-1}X}(\cos v)^\alpha dv. \tag{8}$$

These models were fit to the data using the KS test to measure the quality of a fit, as described in Section 2.3. The best-fit value of s is 3.5 with a 90 per cent confidence range $3.28<s<4.1$. $X_\odot$ varies between 3 and 20 through this range but is highly correlated with s. At $s=3.5$, $X_\odot\approx 8.6$ with a 90 per cent confidence range $5.7<X_\odot<11.2$.

3.2 THREE-DIMENSIONAL DISTRIBUTION

The rest of the analysis is restricted to the 147 globular clusters with distance estimates. Fig. 5 shows the projections of their positions on to the x–y and x–z planes (the y–z projection is similar to the sky distribution shown in Fig. 2). It is immediately apparent that there is a bar-like extension along the x-axis and this was reported in many early papers as strong evidence for flattening. However, as we showed in Section 3.1 the sky distribution contains no such feature and as pointed out by Woltjer (1975) much or all of the effect may be due to distance errors.

We can characterize the distributions along each axis by the cumulative number distribution. The centroid is measured using the median; the mean is sensitive to data errors and gives high weight to the points at large distance from the Galactic Centre. The range of allowable positions for the median is found as follows: consider different positions for the median. We would reject these if there is too large an excess of clusters to either side of this position. The distribution is approximately normal with mean 147/2 and variance 147/4 so that a two-sided test rejects models which give more than $(1.65\times\sqrt{147}+147)/2\approx 83\frac{1}{2}$ clusters to one side of the median. The positions of the 64th and 84th clusters in the cumulative distribution thus define the 90 per cent confidence range. The results are shown in Table 2.

Next we compare the distribution with that obtained by a point reflection through the centroid (this is a two-sided KS test with 73 points). The results, given in Table 2, are consistent with a symmetric distribution. The data are then folded on to $|x-7.07\text{ kpc}|$, $|y|$ and $|z|$ to compare the different coordinate directions. $|y|$ and $|z|$ are consistent with being drawn from the same distribution with probability 0.89 but $|x-7.07\text{ kpc}|$ and $|y|$ only at probability

Table 2. This table shows for each of the three coordinate directions the position of the median, the 90 per cent confidence range in this position and the probability that the distribution is symmetric about the median.

	median	90% range		sym
x	7.07	6.21	7.75	0.28
y	0.01	−0.53	0.26	0.20
z	−0.01	−0.48	0.40	0.64

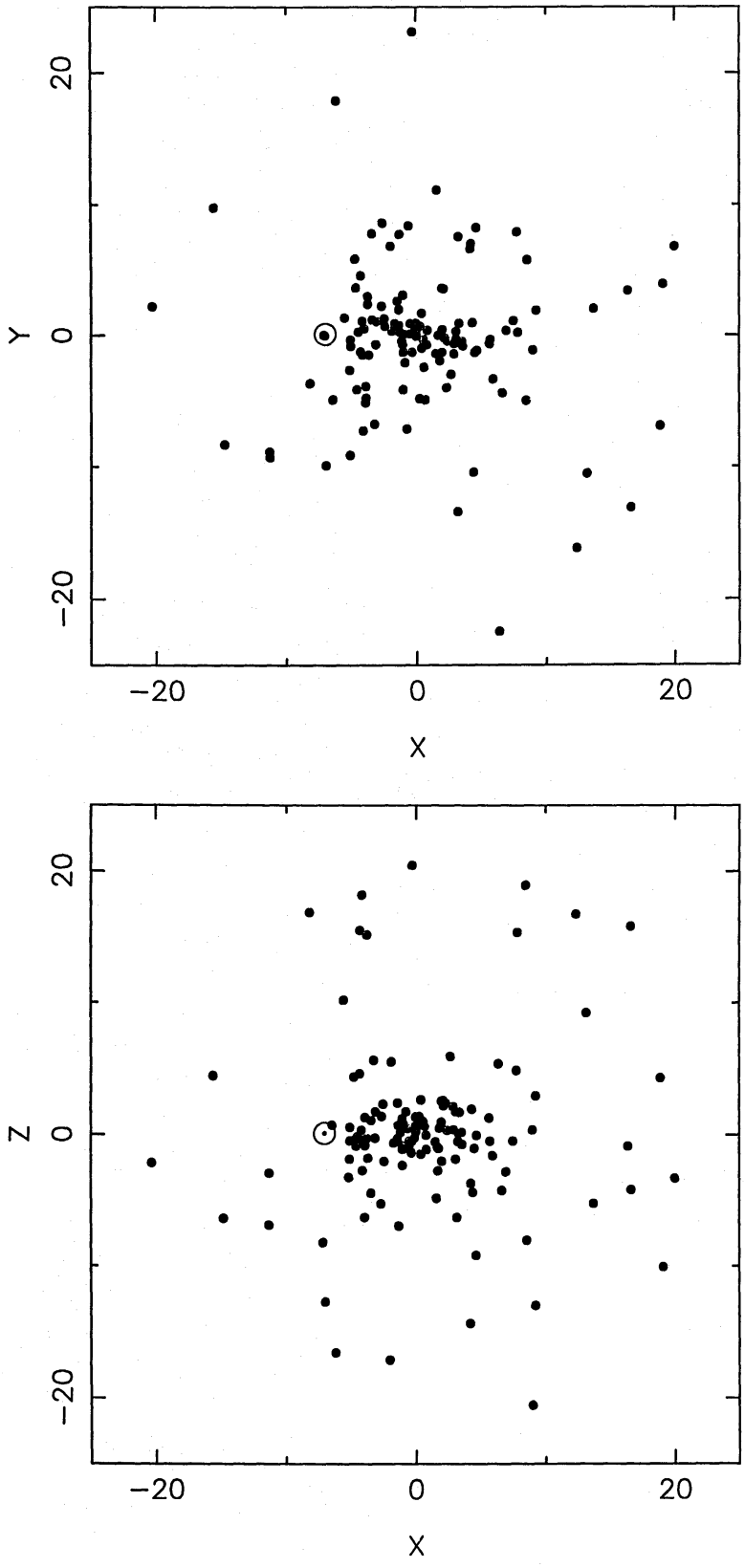

Figure 5. Those globular clusters with distance estimates projected along the y- and z-axes, out to 25 kpc either side of the Galactic Centre. The Sun's position is shown as an open circle.

3×10^{-3} and $|x-7.07\,\mathrm{kpc}|$ and $|z|$ at probability 7×10^{-3}. This confirms what the eye tells us – that the distribution is significantly more extended in the x-direction than along the other two axes.

Two things can affect the observed distribution:

(i) Obscuration will cause incompleteness of the sample, primarily behind the Galactic Centre. The medium will be shifted towards us and symmetry will be destroyed.

(ii) Distance errors will cause an extension towards the Galactic Centre, such as is observed, and systematic errors could lead to an incorrect distance estimate for the median which would not be detectable from the globular cluster sample alone. Table 3 shows the position of the median for various cuts in z of the data, together with the probability that the distribution in x is symmetric. There is a slight shift of the median to higher x away from the galactic plane but this is not significant and the symmetry is not destroyed. Thus there is little internal evidence in the globular cluster sample for extensive obscuration causing incompleteness in the galactic plane. This effect is present at some level as some new clusters are still being found (e.g. Djorgovski 1988). Also, the median distance of 7.07 kpc is much lower than that determined by most other methods. For this reason the IAU recommended value of 8.5 kpc is used for comparison in the following sections.

The 36 high-metallicity clusters have median $x=7.20$ kpc with range 6.40 to 9.52 but are symmetrically distributed about this with a probability of only 2×10^{-2}. They are distributed in the same manner as the total sample with probability 0.19. The metal-poor subsample is biased to lower distances but this is mainly due to the omission of 11 clusters with unknown metallicities, all but one of which lie beyond 7.07 kpc. When these are included the sample median is 6.19 kpc with 90 per cent range 5.17 to 7.37. Neither of these subsamples show a significant variation of the median distance with height above the galactic plane. It is because the distances to many of these distant clusters were only recently determined that our results are contrary to the conclusions of FW82 who found a significant shift between the medians of the metal-rich and metal-poor subsamples, with the former lying at a greater distance. They attributed this to an increase in the absolute magnitude of the horizontal branch with metallicity (Christy 1966; Sandage 1982); the above data show only slight evidence for such an effect.

The observed cumulative number distribution along each axis can be used, in much the same way as for the angular distribution, to constrain models of the space density. We use the same models $\rho\propto[1+(R/a)^2]^{-s/2}$ except that now we have to introduce an outer cut-off; there are no clusters observed beyond $R=120$ kpc even though we should expect about 10 on a simple extrapolation. The cumulative distribution then becomes

$$\Psi(y)=\frac{N}{2}\left[1+\frac{I_{s-4}(y/a)}{I_{s-4}(100/a)}\right], \tag{9}$$

Table 3. Properties of the x-distribution of globular cluster positions for various cuts with distance, $|z|$, from the galactic plane, $N(>z)$ and $N(<z)$ give the number of clusters at distances greater and less than z kpc from the plane, respectively. The other columns are as in Table 2.

z	$N(>z)$	median	90% range		sym	$N(<z)$	median	90% range		sym
0.0	147	7.07	6.21	7.75	0.28					
0.5	121	7.07	6.07	8.57	0.51	26	7.00	5.78	8.68	0.88
1.0	98	7.48	6.05	9.06	0.86	49	6.78	6.01	7.32	0.90
2.0	75	8.66	5.09	9.41	0.14	72	7.00	6.27	7.41	0.88
3.0	58	7.73	3.64	11.5	0.56	89	7.07	6.45	7.48	0.32

Table 4. Best fit values and the 90 per cent confidence range for parameters describing the spatial distribution of clusters with angle, ω, from the Galactic Centre and along each coordinate axis. The core radii inferred from the angular distribution are proportional to the distance, g, from the Sun to the Galactic Centre; the values listed here are for $g = 7.07$ kpc.

	Best fit		90% range				90% range of a for $s = 3.5$	
	s	a	s		a			
ω	3.5	0.82	3.28	4.1	0.35	2.4	0.63	1.3
X	4.5	4.99	3.30	>7	1.05	>10	1.6	2.2
y	3.5	1.17	3.15	4.5	0.27	3.5	0.83	1.6
z	3.5	1.16	3.15	4.7	0.37	3.7	0.73	1.6

where, to include all the data, a one-dimensional cut-off of 100 kpc has been chosen – the exact value does not matter. As the distribution is symmetric the data are folded on to $y > 0$ to improve the statistics. The results for y and z (shown in Table 4) agree well with those inferred from the angular distribution. The core radii are slightly larger (for a distance to the Galactic Centre of $g = 7.07$ kpc) but the two are compatible at the 50 per cent level. The distribution in X gives very different results: the best-fit value of s is increased to 4.5 but only values smaller than 3.3 can be excluded. For a given s, however, the core radius is much larger, has a smaller allowable range and with $s = 3.4$ is incompatible with the results for the other two co-ordinate axes and for the angular distribution. The ratio of core radii suggests that the x-distribution is 'stretched' by a factor of 1.6 or more.

Consider the effect of distance errors, in particular the simple form in which the observed magnitude, m, lies uniformly in the interval $[m_0 - \Delta m, m_0 + \Delta m]$ about the true magnitude m_0. This error does not alter expected median position of a single object; the sample median is biased slightly towards the Sun but this effect turns out to be small (see Fig. 6). The errors can be described by a function, $e'(m - m_0) = (2\Delta m)^{-1}$, $-\Delta m < m - m_0 < \Delta m$, which must be

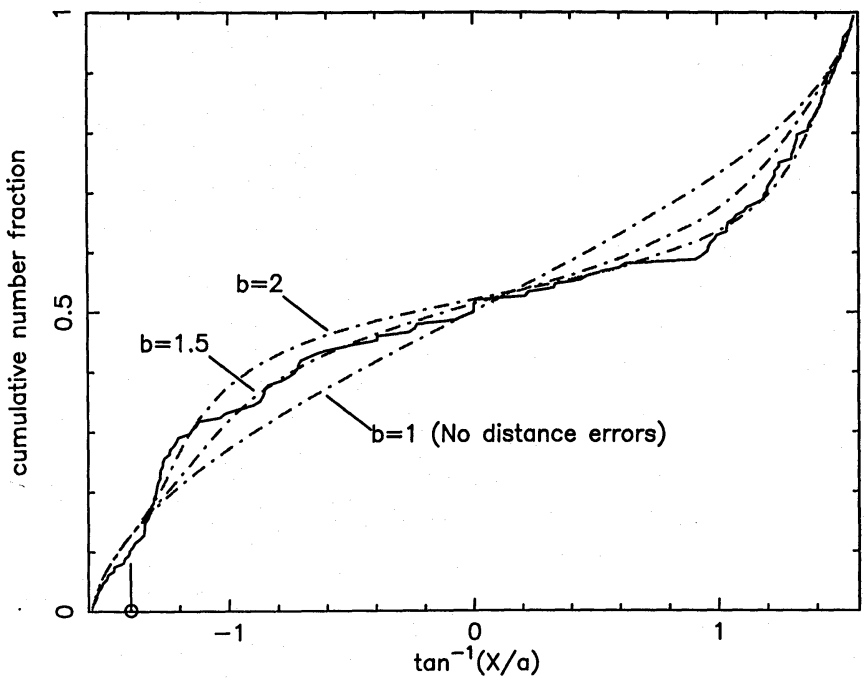

Figure 6. The distribution of globular clusters along the x-axis together with models as described in the text. The Sun's position is also shown.

convolved with the true distance distribution to get the observed one. The inferred distance, d, of a cluster is related to the real distance, d_0, by $d = d_0 10^{-(m-m_0)/5}$. Writing $d = d_0\eta$, we have for the error in distance $e(\eta) = (2\eta \ln b)^{-1}$, $1/b < \eta < b$ where $b = 10^{\Delta m/5}$. Note that the error in one co-ordinate direction does not depend upon the displacement along the other two axes. The observed strip count, $\tilde{\psi}$, in the y and z directions is related to the true strip count, ψ, by

$$\tilde{\psi}_y(y)\,dy = \int_{1/b}^{b} \psi\left(\frac{y}{\eta}\right)\frac{dy}{\eta}\,e(\eta)\,d\eta, \tag{10}$$

which gives a cumulative number distribution

$$\tilde{\Psi}_y(y) = \frac{1}{2\ln b}\int_{-\infty}^{y} \frac{\Psi(by') - \Psi(y'/b)}{y'}\,dy'. \tag{11}$$

The central strip count density given by equation (11) as $y \to 0$ is $\tilde{\psi}(0) = (b - 1/b)/(2\ln b)\,\psi(0)$. The multiplicative factor in front of $\psi(0)$ is only 1.08 even for b as large as 2, and the overall effect on the distribution is negligible. The situation for the x-direction is different because of the displacement:

$$\tilde{\psi}_X(X)\,dX = \int_{1/b}^{b} \psi\left(\frac{X+g}{\eta} - g\right)\frac{dX}{\eta}\,e(\eta)\,d\eta, \tag{12}$$

giving

$$\tilde{\Psi}_X(X) = \frac{1}{2\ln b}\int_{-\infty}^{X} \frac{\Psi[bX' + (b-1)g] - \Psi[X'/b + (1/b - 1)g]}{(X' + g)}\,dX'. \tag{13}$$

As b increases the distribution becomes skew with the maximum value of $\tilde{\Psi}$ being lowered (until b increases beyond about 3) and shifted towards the Sun. Fixing s and a at the best-fit values previously found then b can be varied to find an acceptable fit. The 90 per cent confidence range for $s = 3.5$, $a = 0.82$ (from the angular distribution) has $b > 2$ but with only a narrow range, indicating a poor fit. If a is increased to 1.16 as suggested by the y and z distributions then $1.5 < b < 2.3$ (see Fig. 6) – these results agree with the naive estimate given above and with Monte Carlo simulations carried out by FW82. $b = 1.5$ corresponds to $\Delta m = 0.88$ (or a variance of ≈ 0.5 mag) which is reasonable for the sample as a whole but is much greater than the errors in the best data points. Unfortunately the subsample of clusters with good distance estimates is strongly biased to the near side of the Galactic Centre and so is subject to severe selection effects; as noted above, however, the distribution does look symmetrical about the median. A recent study by Armandroff (1988) gives colour-magnitude diagrams for six metal-rich globular clusters. In five cases the level of the horizontal branch differs by more than one magnitude from previous, secondary estimates. In view of the inhomogeneity of the sample and the uncertainties in the reddening estimates it is probably reasonable to attribute all the observed extension in spatial distribution to distance errors – otherwise the globular cluster system contains a bar several kiloparsecs long pointing within about 10° of the direction of the Sun!

To summarize this section: the distribution of metal-poor clusters on the sky is circularly symmetric about the Galactic Centre but becomes flattened towards the galactic plane for metal-rich systems. Together with the assumption of spherical symmetry, the sky distribution can be used to constrain a simple two-parameter model for the space distribution of the

clusters. Incompleteness of the sample due to obscuration may be present but does not manifest itself in an obvious way. The errors in distance and metallicity are large and render suspect any results which depend upon the observed displacement towards the Galactic Centre.

4 Rotation

The analysis described here follows closely that described in Frenk & White (1980, hereafter FW80). The observed radial velocity, $v_{\mathrm{obs},i}$, of a globular cluster is composed of several parts:

$$v_{\mathrm{obs},i} = -(\mathbf{v}_{\mathrm{lsr}} + \mathbf{v}_{\odot})\cdot\hat{\mathbf{r}}_i + v_{\mathrm{rot}}(R_i)\cos\psi_i + v_{\mathrm{pec},i}, \tag{14}$$

where v_{rot}, the rotation velocity, is a function of galactocentric distance, R_i, $\cos\psi_i$ is the angle between the rotation vector and the line-of-sight (see Fig. 1) and $v_{\mathrm{pec},i}$ is the random velocity due to the velocity dispersion (and errors). Initially we take the local standard of rest to have a velocity, $\mathbf{v}_{\mathrm{lsr}}$, of 220 km s^{-1} along the y-axis and the Sun's motion relative to this, $\mathbf{v}_{\odot}$, to be 20 km s^{-1} towards $b = 22°$, $l = 57°$; variations in v_{lsr} will be discussed below. For the purposes of the fits to v_{rot}, the velocity dispersion is supposed both isotropic and independent of radius; as is shown in the next section this assumption does not hold but it is unimportant here. Writing v_i for the 'corrected' velocity $v_i = v_{\mathrm{obs},i} + (\mathbf{v}_{\mathrm{lsr}} + \mathbf{v}_{\odot})\cdot\hat{\mathbf{r}}_i$ and taking as an example $v_{\mathrm{rot}} =$ constant then equation (14) can be solved for v_{rot} to give

$$v_{\mathrm{rot}} = \frac{\Sigma v_i w_i}{\Sigma\cos\psi_i w_i} - \frac{\Sigma v_{\mathrm{pec},i} w_i}{\cos\psi_i w_i}, \tag{15}$$

where the w_i are arbitrary weighting factors. The variance of the rotation estimate is

$$\mathrm{var}(v_{\mathrm{rot}}) = \frac{\Sigma w_i^2}{(\Sigma w_i\cos\psi_i)^2}\,\mathrm{var}(v_{\mathrm{pec},i}). \tag{16}$$

Minimizing over each of the w_i's we find $w_i \propto \cos\psi_i$ and so the minimum variance estimate for v_{rot} is given by

$$v_{\mathrm{rot}} = \frac{\Sigma v_i\cos\psi_i}{\Sigma\cos^2\psi_i} \pm \sqrt{\frac{\mathrm{var}(v_{\mathrm{pec},i})}{\Sigma\cos^2\psi_i}}. \tag{17}$$

This method can be extended to include a radial expansion term in the globular cluster motion. For example, taking a constant expansion, v_{exp}, everywhere leads to

$$v_{\mathrm{rot}} = \frac{\Sigma v_i\cos\psi_i\Sigma\cos^2\phi_i - \Sigma v_i\cos\phi_i\Sigma\cos\psi_i\cos\phi_i}{\Sigma\cos^2\psi_i\Sigma\cos^2\phi_i - (\Sigma\cos\psi_i\cos\phi_i)^2} \tag{18}$$

$$v_{\mathrm{exp}} = \cos\psi_i \leftrightarrow \cos\phi_i,$$

although the variance in this case is more difficult to evaluate. The $\Sigma\cos\psi_i\cos\phi_i$ term becomes relatively unimportant as the number of clusters is increased, which is probably why FW80 omitted it from their equation (4). Because v_{rot} is often much greater than v_{exp}, however, this term should be included when calculating the latter, especially for small datasets.

Test datasets have been used, as described in Section 2.4, to check the above method. Both the mean and variance of v_{rot} are reproduced well. The velocity dispersion is also returned correctly for isotropic orbits with the fractional variance being approximately equal to the

inverse number of clusters. Radial and tangential orbits give smaller velocity dispersions, since we are only seeing the projection on to the position vector, and have larger variances. Distance errors of a factor of 2 (see Section 3.2) increase the estimated rotation speed and velocity dispersion by about 10 per cent. Taking too small a distance to the Galactic Centre (e.g. 7 kpc instead of 8.5 kpc) has a similar but slightly more pronounced effect. The reason for these changes is simply that errors in position tend to move clusters away from $\psi \approx 0°$ to lower values of $\cos\psi$. It is difficult to disentangle the effects of an incorrect choice of $v_{\rm lsr}$ from the rotation, as $\cos\psi$ and $\hat{\mathbf{r}}\cdot\hat{\mathbf{y}}$ are similar over much of space. If $v_{\rm lsr}$ is decreased the measured rotation is increased by about the same amount at large radii but by only a little near the Galactic Centre.

The variance obtained from the fitting procedure shows the allowable range of parameters but does not indicate how well the model fits the observations. It is possible to look for trends of the residual velocity, $v_{{\rm res},i} = v_i - v_{\rm rot}\cos\psi_i - v_{\rm exp}\cos\phi_i$, with either $\cos\psi$, $\cos\phi$ or R. In practice we find that this gives constraints similar to those inferred above. The data can also be subdivided into radial bins and fit separately within each although the errors become larger in this case.

The best-fit constant rotation model for the whole sample is $v_{\rm rot} = 65 \pm 18$ km s^{-1}. This is consistent with that deduced within each of the radial subdivisions listed in Table 5 and shows no trends with $\cos\psi$, $\cos\phi$ or R. The best-fit solution with a constant expansion velocity gives $v_{\rm exp} = 5 \pm 14$ km s^{-1} and leaves $v_{\rm rot}$ virtually unchanged. Fig. 7 shows the residuals for this fit plotted on the $R - \cos\psi$ plane. Clearly there is little power in the high R clusters to determine the rotation velocity. The lines show the effect on the positions in this plane of distance errors which, as discussed above, have little effect on the inferred value of $v_{\rm rot}$.

Even though the data are consistent with a constant rotation velocity the best-fit rotation to the outer radial bin is smaller than for the inner two; models in which the whole system rotates at this lower speed show strong residual trends with $\cos\psi$ and so can be rejected. We have also

Table 5. Parameter estimates for the rotation models described in the text. $\sigma_{\rm los}$ km s^{-1} is the residual line of sight velocity dispersion.

Sample	N	v_{rot}	v_{exp}	σ_{los}
All	115	66 ± 18	5 ± 14	110
		65 ± 18	—	110
$R < 3.5$	38	69 ± 25	34 ± 30	106
		65 ± 25	—	108
$3.5 < R < 7$	31	103 ± 25	38 ± 19	79
		91 ± 26	—	83
$R > 7$	46	29 ± 46	-16 ± 21	124
		28 ± 47	—	125
All *	115	95 ± 29	4 ± 14	111
		95 ± 29	—	111
Metal-rich	31	119 ± 25	50 ± 20	83
		113 ± 27	—	91
Metal-poor	84	42 ± 23	10 ± 16	114
		43 ± 23	—	114
$R < 3.5$	24	60 ± 32	-1 ± 38	110
		61 ± 32	—	110
$3.5 < R < 7$	19	44 ± 30	23 ± 25	76
		39 ± 31	—	78
$R > 7$	41	19 ± 49	21 ± 23	129
		19 ± 50	—	130

*This sample was analysed with a different model – see text.

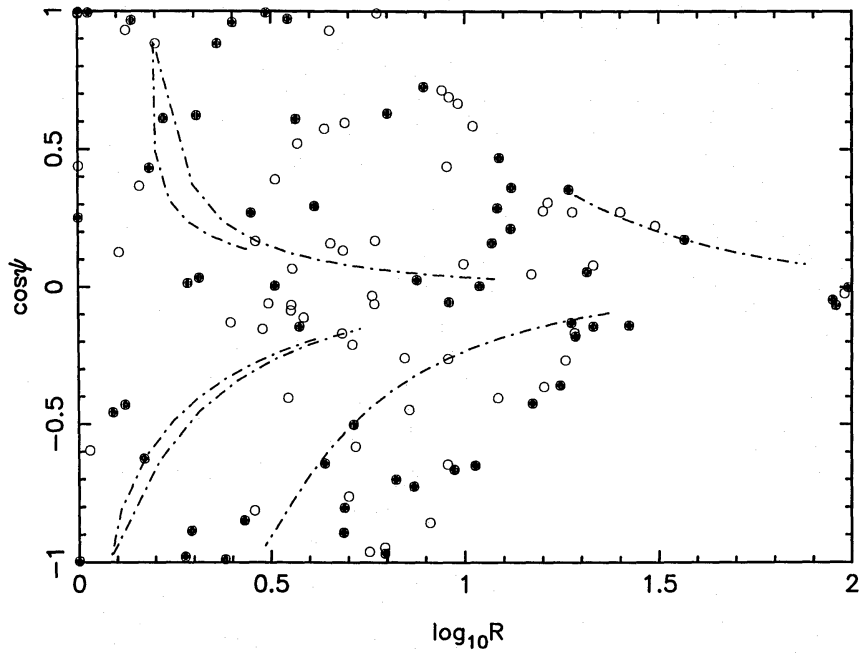

Figure 7. The residuals of the best fit constant rotation model plotted in the $R-\cos\psi$ plane. Those clusters with $R<1$ kpc have been plotted at $R=1$ kpc. The filled circles and open circles represent negative and positive velocities, respectively. The lines show the effect of distance errors on the positions in this plane of four representative clusters.

fit the data with a model in which the rotation velocity is given by $v_{\rm rot}[1+(X^2+Y^2)]^{-1/4}$, which is asymptotically Keplerian. This fits the data just as well as the constant rotation model, which emphasizes how weak the constraints are. Solid body rotation is, however, ruled out.

The results obtained by treating all the data together are unsatisfactory, especially as there is evidence for a spatial distinction between the metal-poor and metal-rich systems. The picture is clarified when these are treated separately. The metal-poor system is found to be slowly rotating and while it does show a decrease in rotation velocity outwards the errors are such that this is not significant. The metal-rich globular clusters, on the other hand, are fast-rotating and show a significant expansion velocity; a zero expansion solution shows trends with $\cos\phi$ at the 3 per cent level. This implies that there are streaming motions over and above those due to the rotation although it is not necessary that a true spherically symmetric expansion be taking place. A similar effect was noted by Clube & Watson (1979) for a sample of 29 globular clusters with projected positions close to the Galactic Centre. The metal-rich clusters also have a smaller line of sight velocity dispersion than the metal-poor ones although once again the significance of this difference is small. We have looked for a sharp transition from fast to slow rotation as the metallicity is varied. There does apear to be a transition at [Fe/H] $=-1.0$ but the errors are such that it is not significant. Clearly metallicity errors will cause a blending of metal-rich and metal-poor populations, confusing the issue and a more definite statement must await more accurate observations. The above results are in agreement with Z85, HSW and AZ88.

If the data are treated as a whole then there are signs of residual motions once the best fit rotation model has been 'subtracted' off. Of the 38 clusters in $R<7$ kpc only 14 have residual positive motions while, of the 31 clusters in 3.5 kpc $<R<7$ kpc, 21 have positive residuals. Assuming a random distribution these results are 1.6 and 2.0 sigma, respectively. This conclusion becomes much less certain when the metal-rich and metal-poor clusters are fit separately. Only 11 of the 31 metal-rich globular clusters have positive residual velocities but

21 of them have $l<0°$. Thus it is possible that a combination of obscuration and incorrect rotation velocity could lead to the observed result. Expansion about too near a Galactic Centre position, due to obscuration of distant clusters, would also have this effect.

Rodgers & Paltoglou (1984) suggest that there is at least one distinct subgroup of globular clusters with metallicities in the range $-1.3>[\mathrm{Fe/H}]>-1.7$ which has a significantly different rotation velocity from the mean. We have performed a similar analysis and find less extreme variations in velocity than they do, and well within the expected uncertainties. This is partly due to different metallicities which shift two of their clusters with high retrograde motions out of the metallicity range given above. Once again more accurate metallicities would be useful.

5 Velocity dispersion

5.1 OBSERVATIONS

The analysis follows closely that of FW80 but the conclusions differ slightly – principally because a wider range of models is considered. The best-fit rotation model is first subtracted from the data (the results are not very sensitive to the exact form used for the rotation) and the residual velocities are then to be explained as being drawn from a normal distribution with mean 0 and dispersion $\sigma_i^2(\mathbf{R}_i)$. Models are rejected if $v_{\mathrm{res},i}^2/\sigma_i^2(\mathbf{R}_i)$ shows trends with R or $\cos^2\phi$ – recall that ϕ is the angle between the line-of-sight to the cluster and the radius vector from the Galactic Centre. We check for trends within subdivisions of the data as well as in the data as a whole. We do not combine trend tests with R and $\cos\phi$ as in FW80 (see Section 2.3).

The velocity dispersion is assumed to be ellipsoidal with one-dimensional components σ_R^2 along the radial direction and σ_T^2 in each of the perpendicular axes – this may not be a good assumption for the metal-rich clusters. The eccentricity, e, is defined as $\sigma_R^2/3\sigma^2$, where $3\sigma^2=\sigma_R^2+2\sigma_T^2$; a value of $e=\frac{1}{3}$ indicates isotropy. The projected velocity dispersion along the line-of-sight is

$$\sigma_i^2=\sigma_e^2+\sigma_R^2\cos^2\phi_i+\sigma_T^2\sin^2\phi_i=\sigma_e^2+\sigma^2[(3\cos^2\phi_i-\tfrac{3}{2}\sin^2\phi_i)e+\tfrac{3}{2}\sin^2\phi_i], \tag{19}$$

where σ_e^2 is the observational error.

The maximum likelihood estimators for σ_R^2 and σ_T^2 are

$$\begin{aligned}\mathrm{mle}(\sigma_R^2)&=\frac{\Sigma A_i(v_{\mathrm{res},i}^2-\sigma_e^2)\cos^2\phi_i\Sigma A_i\sin^4\phi_i-\Sigma A_i(v_{\mathrm{res},i}^2-\sigma_e^2)\sin^2\phi_i\Sigma A_i\cos^2\phi_i\sin^2\phi_i}{\Sigma A_i\cos^4\phi_i\Sigma A_i\sin^4\phi_i-(\Sigma A_i\cos^2\phi_i\sin^2\phi_i)^2}\\ \mathrm{mle}(\sigma_T^2)&=\cos\phi_i\leftrightarrow\sin\phi_i,\end{aligned} \tag{20}$$

where $A_i=1/\sigma_i^4$ contains σ_R^2 and σ_T^2 so that the system must be solved iteratively. If A_i is fixed at the best-fit value then the variance of the estimator can be evaluated. It is possible instead to solve for e and σ^2 in an analogous manner to equation (20). This gives similar results where the data are sufficient to constrain e closely but otherwise e and σ^2 become strongly coupled.

The simulated data of Section 2.4 were used to test these estimators. Strongly radial or strongly tangential datasets return the correct eccentricities with only a small scatter but isotropic datasets are not well constrained. For example isotropic distributions of 40 particles in $R<3.5$ kpc or $3.5\,\mathrm{kpc}<R<7$ kpc gave $e\approx0.32\pm0.17$ (formal 1σ error assuming a Gaussian distribution) with extreme values of 0 and 0.84. The velocity dispersion is distributed about the correct value with errors similar to those derived from equation (20). Distance errors have a large effect on the inferred values of $\cos^2\phi_i$ and so tend to isotropize the observed velocity dispersion. For example in $R<3.5$ kpc radial orbits give $e=0.64\pm0.25$ and tangential orbits $e=0.28\pm0.22$ with extreme values ranging between 0 and 1 in each case.

These estimators have been applied to various cuts of the data with the results shown in Table 6 – the observational error, σ_e^2 has been set to zero. Fig. 8 shows the globular clusters plotted on the $R-\cos^2\phi_i$ plane. It is clear that for $R>7$ kpc there is little power to determine the eccentricity. Only if the distance errors are small in the range $3.5\,\text{kpc}<R<7\,\text{kpc}$ where most of the clusters are at high galactic latitude will the eccentricity be well defined; the value of 0.30 ± 0.12 from Table 6 is consistent with isotropy.

The line-of-sight velocity dispersion is smaller at radii less than 7 kpc than at larger radii – this holds regardless of the rotation model. The errors in the velocity determinations of the outer clusters are probably larger than for the inner ones but this is unlikely to account for more than a small part of the difference. The radial component of the velocity dispersion must therefore increase outwards although the total velocity dispersion need not. The difference in velocity dispersion between the $R<3.5$ kpc and $3.5\,\text{kpc}<R<7\,\text{kpc}$ bins is not significant; distance errors will increase the observed central dispersion slightly.

Table 6. Maximum likelihood estimates for the velocity dispersion in units of $(100\,\text{km s}^{-1})^2$. In each case the best fit constant rotation model has been subtracted from the data, except * which also includes an expansion term.

Sample	N	σ^2_{obs}	σ^2_R	σ^2_T	σ^2	e
All	115	1.21	1.21 ± 0.23	1.20 ± 0.29	1.22 ± 0.16	0.33 ± 0.07
$R<3.5$	37	1.17	0.92 ± 0.51	1.28 ± 0.38	1.16 ± 0.27	0.27 ± 0.15
$3.5<R<7$	32	0.69	0.64 ± 0.25	0.75 ± 0.31	0.71 ± 0.18	0.30 ± 0.12
$R>7$	46	1.56	1.40 ± 0.37	2.23 ± 1.32	—	—
Metal-rich *	31	0.69	0.41 ± 0.17	1.03 ± 0.39	0.82 ± 0.21	0.17 ± 0.07
Metal-poor	84	1.30	1.31 ± 0.30	1.31 ± 0.38	1.31 ± 0.20	0.33 ± 0.08
$R<3.5$	24	1.21	0.47 ± 0.45	1.56 ± 0.54	0.98 ± 0.21	0.18 ± 0.10
$3.5<R<7$	19	0.61	0.59 ± 0.32	0.61 ± 0.32		
$R>7$	41	1.69	1.58 ± 0.45	2.08 ± 1.35	—	—

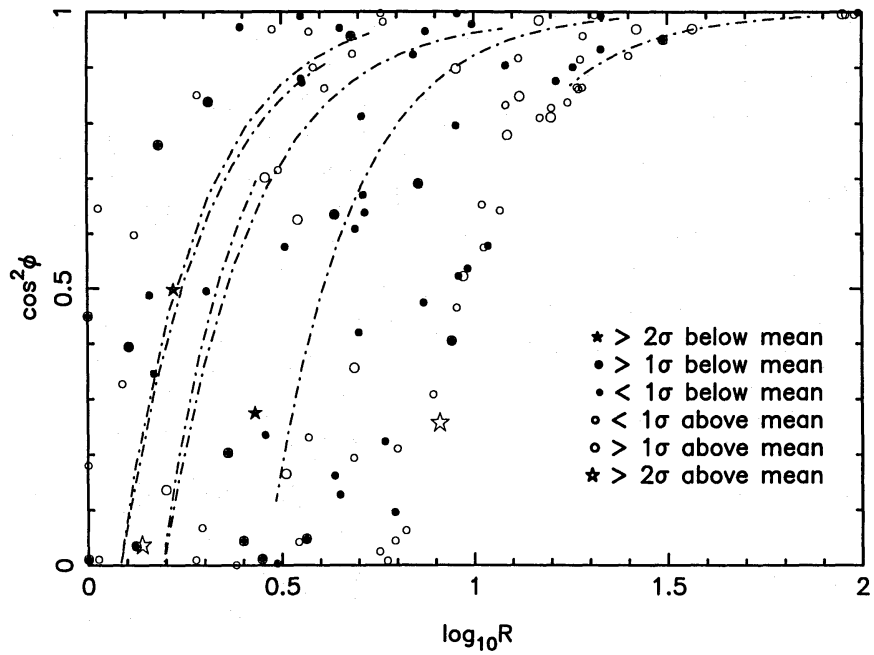

Figure 8. The residuals of the best fit constant rotation model plotted in the $R-\cos^2\phi$ plane. The different symbols show the relative magnitudes of the square of the observed velocities; there is a clear increase in velocity dispersion with radius. The lines show the effect of distance errors on the positions in this plane of four representative clusters.

This is essentially all the information which can be extracted from the observations. We wish to find the constraints which these impose on the mass of the Galaxy. To do this a range of models for the velocity dispersion are fit to the data and then used to determine the galactic rotation speed $V_c(R)=\sqrt{GM(R)/R}$. No account is taken of the effect of distance or velocity errors: thus the models are likely to be over-restrictive, especially with regard to eccentricity. Also, the metal-rich and metal-poor samples are analysed together in order to improve the statistics.

5.2 MODELS

(i) The simplest model to consider is one in which the eccentricity is constant and the normalization varies as a power law with radius, $\sigma^2=\sigma_0^2 R^\alpha$, $e=$constant. We know immediately from Table 5 that e must be close to $\frac{1}{3}$ in order to satisfy the constraints in $R<7$ kpc and that α will have to be positive so that σ^2 increases outwards. This is indeed what we find; the results are summarized in Fig. 9(a). These conclusions agree with those of FW80. A constant velocity dispersion, constant eccentricity model is at best marginally consistent with the data at the 4 per cent level.

(ii) The next step is to consider models with more freedom in the eccentricity. FW80 chose to allow σ_R^2 and σ_T^2 to vary independently as power laws in radius. This allows the eccentricity to vary also, but the restriction imposed by the data that $e\approx\frac{1}{3}$ in $R<7$ kpc then renders unacceptable any model in which the motions become highly radial in the outer regions. It is for this reason that they conclude that both σ^2 and V_c are either constant or increasing outward. We choose instead to look at models of the form $\sigma_T^2=\sigma_R^2/[1+(R/c)^2]$ as have been described by Merritt (1985). These models are similar to those discussed by White & Frenk (1983). They are isotropic in the centre and then become increasingly radial at radii greater than c. We consider a family of models $\sigma_R^2\propto(c^2+R^2)/(nc^2+R^2)$ ranging from $n=1$, which corresponds to $\sigma_R^2=$constant, to $n=3$, corresponding to $\sigma^2=$constant; the results are shown in Fig. 9(b). Once again all models in which σ_R^2 does not increase outwards are rejected. c must be greater than about 7 kpc in order for the models not to be too radial in 3.5 kpc $<R<7$ kpc, but values up to 30 kpc are acceptable before the velocity dispersion fails to increase fast enough in the outer regions. As Fig. 9(b) shows, there is a reasonable range of parameter space in which models with increasing σ^2 are acceptable at 90 per cent confidence (although none of these models are acceptable at greater than 68 per cent confidence).

(iii) For a given gravitational potential, Merritt gives the equation satisfied by the velocity dispersion (his equation 18). This has been used to construct the velocity dispersion model corresponding to the mass distribution $M\propto R$. The rotation velocity is simply assumed to give an effective mass $M-Rv_{\rm rot}^2/G$ which will be a good approximation as the correction term is small. Once again a large range of acceptable models is found with 7 kpc $<c<35$ kpc at 90 per cent confidence. Models with an outer cut-off are rejected unless the cut-off radius is similar in extent to the outer clusters in the sample. For example, if the four clusters with $R>50$ kpc are excluded then acceptable models can be found for 7 kpc $<c<25$ kpc and an outer cut-off at 50 kpc, or 7 kpc $<c<14$ kpc and an outer cut-off as low as 25 kpc.

5.3 THE MASS OF THE GALAXY

The velocity dispersion models of the previous section can be used to estimate the mass of the Galaxy. For a distribution of test particles the equations of stellar dynamics give

$$V_c^2=\frac{GM}{R}=v_{\rm rot}^2+\sigma_R^2\left[-\frac{R}{\rho}\frac{d\rho}{dR}-\frac{R}{\sigma_R^2}\frac{d\sigma_R^2}{dR}-2\right]+2\sigma_T^2. \tag{21}$$

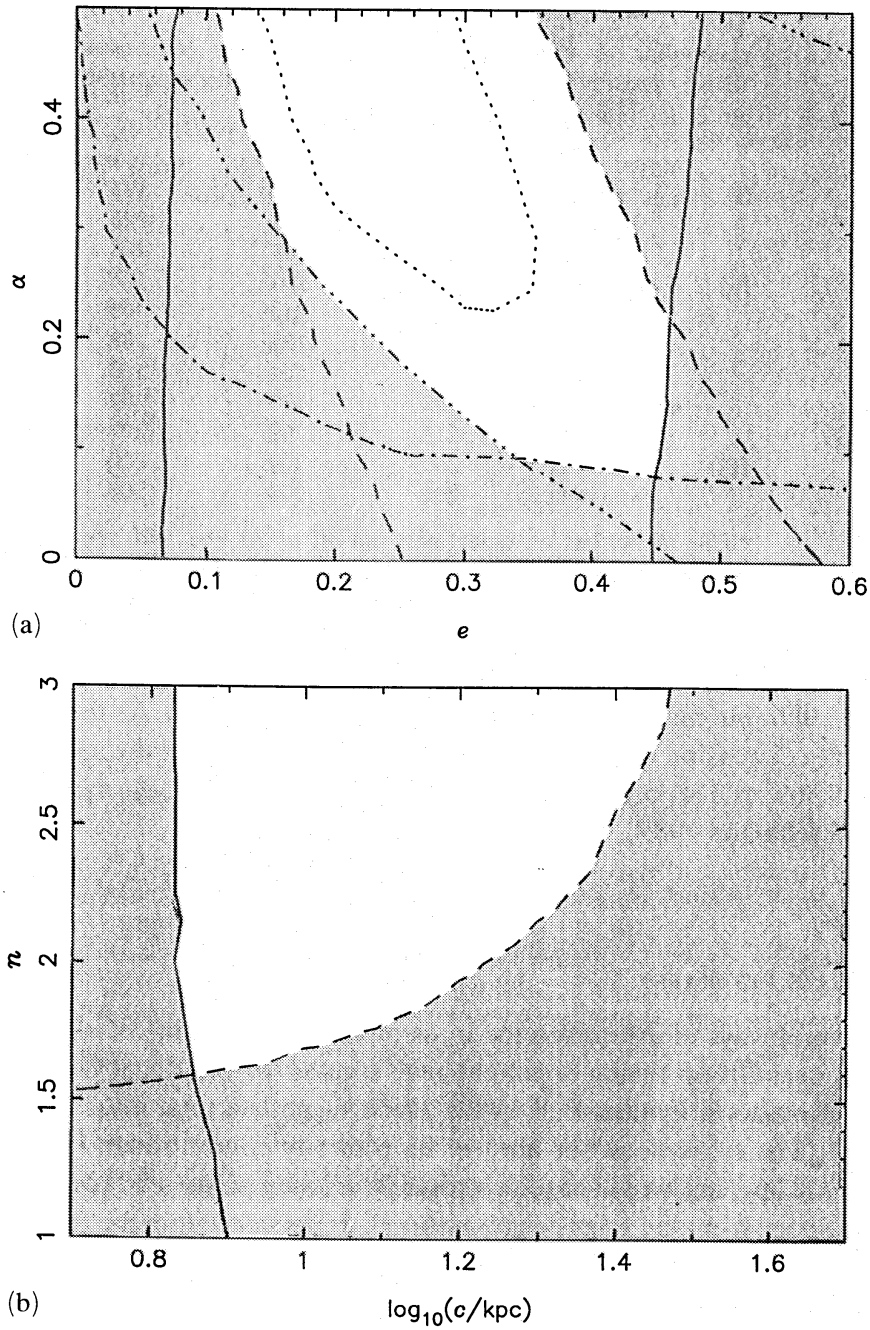

Figure 9. (a) The 90 per cent confidence region for models of the velocity dispersion as described in Section 5.2(i). The various constraints are: solid line, eccentricity in 3.5 kpc $< R <$ 7 kpc; dashed line, eccentricity for all the data; dashed-dotted line, radial variation in $\cos^2\phi > \frac{1}{2}$; dash-dot-dot-dotted line, radial variation in all the data. The dotted line shows the 68 per cent confidence region. (b) The 90 per cent confidence region for models of the velocity dispersion as described in Section 5.2(ii). The constraints are: solid line, eccentricity in 3.5 kpc $< R <$ 7 kpc; dashed line, radial variation in all the data. There is no 68 per cent confidence region in this case.

$-d\ln\rho/d\ln R$ was found in Section 3.1 to be about 3.5; the other quantities are determined by the model. The rotation speed, V_c, is listed in Table 7 for various values of R. Note that for model (iii) we do not need to use equation (21) as the mass is determined *a priori*. For a given model the errors in the mass normalization will be of order $1/\sqrt{N}$ giving an uncertainty of about 5 per cent or 10 km s^{-1} in velocity.

It can be seen from these results that permitted models include those in which the galactic rotation curve is increasing, constant or decreasing with radius. All of the models give rotation

Table 7. The rotation speeds ($km\,s^{-1}$) of the Galaxy corresponding to various models for the velocity dispersion. Those shown in italics give unacceptable fits to the data at 90 per cent confidence.

	Model	V_c(1 kpc)	V_c(7 kpc)	V_c(30 kpc)
(i)	$e=\frac{1}{3}$, $\alpha=0.0$	*215*	*215*	*215*
	$\alpha=0.1$	196	213	228
	$\alpha=0.3$	166	215	263
(ii)	$n=1$, $c=7$	*240*	*207*	*170*
	$c=30$	*217*	*214*	*186*
	$n=2$, $c=7$	205	189	188
	$c=30$	*213*	*211*	*195*
	$n=3$, $c=7$	192	180	201
	$c=30$	211	209	197
(iii)	$c=20$	200	200	200
	* $c=20$	203	203	203

*This model has an outer mass cut-off of 50 kpc, with the four clusters more distant than this being excluded from the analysis.

speeds at the solar radius which lie below the 1985 IAU standard of $220\pm20\,km\,s^{-1}$ (Kerr & Lynden-Bell 1986) but most lie within one standard deviation of it. As the transition radius to a radial velocity dispersion decreases so does the rotation speed at the solar radius. However, even values as low as $180\,km\,s^{-1}$ cannot be ruled out by the current data (e.g. Shuter 1981; Rohlfs & Kreitschmann 1987).

6 Discussion

6.1 OTHER MASS ESTIMATES

There are several ways of estimating the mass of the Galaxy, some of which give conflicting results. The Local Group timing argument gives a mass for the Local Group between 3 and $6\times10^{12}\,M_\odot$ (Einasto & Lynden-Bell 1982) which suggests a total mass for the Galaxy of at least $10^{12}\,M_\odot$. The mass does not have to be centrally concentrated, however, and a halo extending to 200 kpc, say, would require a rotation velocity of just $150\,km\,s^{-1}$. The lower limit to the escape speed from the solar neighbourhood, as deduced from the requirement that high velocity stars be bound, gives a minimum total mass of $5\times10^{11}\,M_\odot$ (Carney & Latham 1986); a similar criterion for the globular clusters in our sample gives just $2\text{–}3\times10^{11}\,M_\odot$ from Eridanus, Pal4, Pal3 and NGC 5694. Peterson (1985) observed five distant clusters and inferred for an isotropic distribution $M\approx5\times10^{11}\,M_\odot$ (the lower limit of $10^{12}\,M_\odot$ which they infer from Eridanus alone is obtained by applying a time-averaged orbit formula to this single datum). Modelling of the Magellanic stream suggests a massive halo which extends to at least 70 kpc or so in order to produce the large infall velocity – this gives a total mass exceeding $\sim8\times10^{11}\,M_\odot$ (Lin & Lynden-Bell 1982). Most recently Little & Tremaine (1987) have done a statistical analysis of the distant satellites of the Galaxy and find a much lower mass $M\lesssim5.2\times10^{11}\,M_\odot$ at 95 per cent confidence, or a rotation speed of less than $165\,km\,s^{-1}$.

As we have shown in this paper, the current globular cluster data are consistent with any of the above mass estimates and are likely to remain so in the foreseeable future. Thus the single piece of evidence that suggests a flat or rising roation curve to large distances remains the modelling of the Magellanic stream. Likewise the only evidence to suggest a decreasing rotation speed at large distances is the low line of sight velocity dispersion of the distant satellites of the Galaxy.

6.2 ECCENTRICITY OF THE VELOCITY ELLIPSOID

It appears from Section 5.2 that the observations exclude orbits which are strongly radial within 7 kpc. Remember however that the distance errors will tend to isotropize the observed velocity dispersion. These orbits also give rotation speeds for the Galaxy at the solar radius which are lower than the currently accepted value of 220 km s^{-1}. The eccentricity of the velocity ellipsoid of old stellar populations in the solar neighbourhood has been extensively investigated; Norris (1987) has reviewed the available data. There are large variations between kinematically and non-kinematically selected samples but even restricting ourselves to the latter σ_R^2 is found to be about $2 \times \sigma_T^2$. This corresponds to an eccentricity of 0.5, or $c \approx g$ in a Merritt model, which is marginally consistent with the above results.

Clearly an independent evaluation of e would be valuable. It was suggested to us that the M31 globular cluster system provides a complementary dataset; for high eccentricity orbits the observed velocity dispersion will decrease outwards along the major axis. Velocity data for M31 has been compiled by Huchra, Stauffer & Van Speybroeck (1982); we exclude B205 and B147 because of the large discrepancy with van den Bergh (1969) and also CFA-1 which seems to have an anomalously low velocity. We divide the data into two samples: the inner clusters at less than 15 arcmin (≈ 3 kpc) from the minor axis and the outer clusters at larger distances. The median velocity is -285 km s^{-1} with a difference between the outer clusters on either side of the minor axis of 141 km s^{-1}. Subtracting off a rotation model which is constant in the outer regions and linear across the inner one, then the velocity dispersions are 104 km s^{-1} for the 24 outer clusters and 123 km s^{-1} for the 32 inner ones. We see only one component of the rotational velocity and for the inner clusters this is likely to vary between 0 and at least 70 km s^{-1}; thus the observed difference in velocity dispersions is not significant. Although it is difficult to draw strong conclusions these data do suggest the distribution of orbits in the M31 globular clusters does not become strongly radial at less than about 3 kpc from the galactic centre – a weak constraint.

6.3 WHAT COULD BE DONE WITH BETTER DATA?

New metallicity and reddening determinations along the lines of AZ88 should lead to a substantial improvement of the data, especially for clusters near the Galactic Centre. This will enable the differences between the metal-rich and metal-poor populations to be investigated in greater detail and will reveal much about the early stages of galaxy formation. More accurate distances would dispel (or confirm!) the possibility of a bar in the spatial distribution and enable the shape of the velocity ellipsoid to be determined out to the solar radius; beyond this, however, it will remain indeterminate due to projection effects. Some radial velocities are still uncertain by 100 km s^{-1} or more and it would be nice to know these more accurately – in particular to determine how much of the increase in velocity dispersion at large radii is real.

Improved data are unlikely, however, to change the general conclusion of Section 5, that a wide variety of mass profiles for the Galaxy are adequate to explain the observed globular cluster phase-space distribution.

6.4 CONCLUSIONS

We have used relatively complete datasets from the literature to investigate the spatial and velocity distribution of the galactic globular cluster population. The distribution as a whole looks circularly symmetric on the sky about the Galactic Centre, but the metal-rich clusters are flattened towards the galactic plane. The sky positions can be used to constrain the core radius

and radial decline of a simple two-parameter model for the spatial distribution; distance data are in general agreement but indicate, in addition, a cut-off at about 100 kpc. We have modelled the distribution of distances towards the Galactic Centre and find that a variance of about 0.5 mag in the measured distance modulus is required to make this consistent with the distributions in the two perpendicular directions.

The rotation of the globular cluster system is only weakly constrained by the data. The best-fit rotation velocity decreases at large radii but the data are consistent with either a constant rotation or Keplerian decline. The metal-rich clusters show a slight tendency to rotate faster and to have a lower velocity dispersion than the mean population. More accurate data are required to determine whether these form distinct sub-populations within the metallicity and phase-space distributions, or whether there is a smooth variation between them.

The velocity dispersion appears isotropic inside the solar radius but this could be largely due to distance errors. The line-of-sight velocity dispersion increases beyond 7 kpc but since the orbits may become radial this provides only a weak constraint on the galactic mass. Models of the velocity dispersion lead to galactic rotation velocities of between about 180 and 220 kpc at the solar radius, which may either rise, remain constant or even decrease at large radii. Low mass models tend to give smaller values for the rotation speed.

Acknowledgments

I would like to thank Carlos Frenk, Dave Hartwick, Doug Richstone and especially Scott Tremaine for many stimulating and useful conversations. This work was supported by the NSERC.

References

Armandroff, T. E., 1988. *Astr. J.*, **96,** 588.
Armandroff, T. E. & Zinn, R., 1988. *Astr. J.*, **96,** 92.
Carney, B. W. & Latham, D. W., 1986. *Dark Matter in the Universe, IAU Symp. No. 117,* p. 39, eds Kormendy, J. & Knapp, G. R., Reidel, Dordrecht.
Christy, R. F., 1966. *Astrophys. J.*, **144,** 108.
Clube, S. V. M. & Watson, F. G., 1979. *Mon. Not. R. astr. Soc.*, **187,** 863.
Djorgovski, S., 1988. Preprint.
Einasto, J. & Lynden-Bell, D., 1982. *Mon. Not. R. astr. Soc.*, **199,** 67.
Freeman, K. C. & Norris, J., 1981. *Ann. Rev. Astr. Astrophys.*, **19,** 319.
Frenk, C. S. & White, S. D. M., 1980. *Mon. Not. R. astr. Soc.*, **193,** 295.
Frenk, C. S. & White, S. D. M., 1982. *Mon. Not. R. astr. Soc.*, **198,** 173.
Hartwick, F. D. A. & Sargent, W. D. W., 1978. *Astrophys. J.*, **221,** 512.
Hesser, J. E., Shawl, S. J. & Meyer, J. E., 1986. *Publs astr. Soc. Pacif.*, **98,** 403.
Huchra, J., Stauffer, J. & Van Speybroeck, L., 1982. *Astrophys. J.*, **259,** L57.
Kerr, F. J. & Lynden-Bell, D., 1986. *Mon. Not. R. astr. Soc.*, **221,** 1023.
Kinman, T. D., 1959. *Mon. Not. R. astr. Soc.*, **119,** 559.
Lin, D. N. C. & Lynden-Bell, D., 1982. *Mon. Not. R. astr. Soc.*, **198,** 707.
Little, B. & Tremaine, S., 1987. *Astrophys. J.*, **320,** 493.
Mayall, N. U., 1946. *Astrophys. J.*, **104,** 290.
Merritt, D., 1985. *Astr. J.*, **90,** 1027.
Norris, J., 1987. In: *The Galaxy, NATO ASI,* p. 297, eds Gilmore, G. & Carswell, R., Reidel, Dordrecht.
Peterson, R. C., 1985. *Astrophys. J.*, **297,** 309.
Rodgers, A. W. & Paltoglou, G., 1984. *Astrophys. J.*, **283,** L5.
Rohlfs, K. & Kreitschmann, J., 1987. *Astr. Astrophys.*, **178,** 95.
Sandage, A., 1982. *Astrophys. J.*, **252,** 553.
Shuter, W. L. H., 1981. *Mon. Not. R. astr. Soc.*, **194,** 851.

van den Bergh, S., 1969. *Astrophys. J. Suppl.*, **19,** 145.
Webbink, R. F., 1981. *Astrophys. J. Suppl.*, **45,** 259.
Webbink, R. F., 1985. *Dynamics of Star Clusters, IAU Symp. No. 113,* p. 541, eds Goodman, J. & Hut, P., Reidel, Dordrecht.
White, S. D. M. & Frenk, C. S., 1983. In: *Kinematics, Dynamics and Structure of the Milky Way,* p. 343, ed. Shuter, W. L. H., Reidel, Dordrecht.
Woltjer, L., 1975. *Astr. Astrophys.*, **42,** 109.
Zinn, R., 1985. *Astrophys. J.*, **293,** 424.